Radiation Physics and Chemistry 212 (2023) 111144

Contents lists available at ScienceDirect

Radiation Physics and Chemistry

journal homepage: www.elsevier.com/locate/radphyschem

Thermoluminescence-based simplified criteria for the detection of irradiated sesame seeds using artificial intelligence methods

J.F. Benavente *, V. Correcher

CIEMAT, Av. Complutense 40, 28040, Madrid, Spain

ARTICLE INFO

Handling Editor: Dr. Chris Chantler

Keywords:
Artificial intelligence
Thermoluminescence
Detection of irradiated food
Initial rise

ABSTRACT

The practical application of unsupervised Artificial Intelligence (AI) numerical methods for analysing unexamined data has gained popularity for solving scientific and technological problems. This paper reports on the implementation of numerical algorithms set based on unsupervised AI methods to discriminate between irradiated and non-irradiated Mexican sesame sample by searching for behaviour patterns in the thermoluminescence (TL) response of polymineral samples adhered to the seeds. Two algorithms were tested, which were able to discriminate between irradiated and non-irradiated samples regardless of whether the whole or initial rise of the TL glow curve was considered. The use of AI algorithms can greatly increase the analytical process by using appropriate models to large datasets. Moreover, free software tools are now available for developers to implement these AI methods in their data analysis code, with Python being the primary language of choice.

1. Introduction

The discrimination of irradiated and non-irradiated samples of Mexican sesame is of great importance due to (i) irradiation is a widely employed food preservation technique that employs ionizing radiation to extend the shelf life of food products and (ii) this process has been proven to be effective in controlling microbial growth and ensuring food safety. It is essential to rely on a methodology to identify irradiated products to uphold consumer rights and ensure proper labelling. Moreover, the international trade of agricultural commodities needs to be controlled by strict regulations, including a proper identification method of irradiated foods. Mexican sesame, being a valuable agricultural product in the region, requires reliable methods to differentiate between irradiated and non-irradiated samples. The accurate determination of irradiation status is crucial for maintaining the quality and integrity of sesame products, preventing fraudulent practices, and complying with regulatory standards. One of the potential methods for the detection of irradiated food is thermoluminescence (TL) that is often used for dose assessment in the fields of ionizing radiation protection dosimetry (El-Faramawy et al., 2023), archaeological and geological dating (Gu et al., 2022) in addition to the detection of irradiated food (Lam et al., 2017; Esmaeili et al., 2023). In this sense, the EN, 1788 standard (2001) provides guidelines for detecting irradiated food by means of the TL properties of mineral phases (quartz, feldspars, clays, etc.) adhered to the seasonings, herbs, spices, vegetables, etc. All these materials show TL properties, i.e. emission of light upon being heated, subsequent to its exposure to ionizing radiation. Such emission is linked to the existence of intrinsic, extrinsic, structural and/or surface defects that are the responsible of the luminescence emission (Mckeever, 1985). The TL process is led by kinetic parameters including activation energy (E), frequency factor (s), and order of kinetics (b), which can be determined by various methods depending on the complexity of the experimental glow curve. One of them, Initial Rise (IR), appear as an easy and quick tool for the TL glow curve analysis and have been used to improve the accuracy and precision of measurements obtained from TL glow curves (Souadi et al., 2022). IR method is based on the calculation of the E value from the initial rise temperature region of the TL glow curve obtained from the slope of a Ln I vs 1/T Arrhenius plot. One of the lacks of IR is that the luminescence efficiency, including the probability of radiative emission and non-radiative transitions, is not considered; i.e. the estimation of the E value by means of IR method used to be underestimated respect to the actual activation energy, although it is not an obstacle to being able to differentiate irradiated and non-irradiated foods (Aramu et al., 1966). The analysis of TL curves by means of IR method has been shown to be a suitable technique for enhancing the discrimination of irradiated foods that contain polymineral phases. This approach can be combined with artificial intelligence (AI) techniques to develop efficient and reliable methods for food safety and quality

* Corresponding author.
E-mail address: jf.benavente@ciemat.es (J.F. Benavente).

https://doi.org/10.1016/j.radphyschem.2023.111144
Received 2 May 2023; Received in revised form 8 June 2023; Accepted 1 July 2023
Available online 3 July 2023

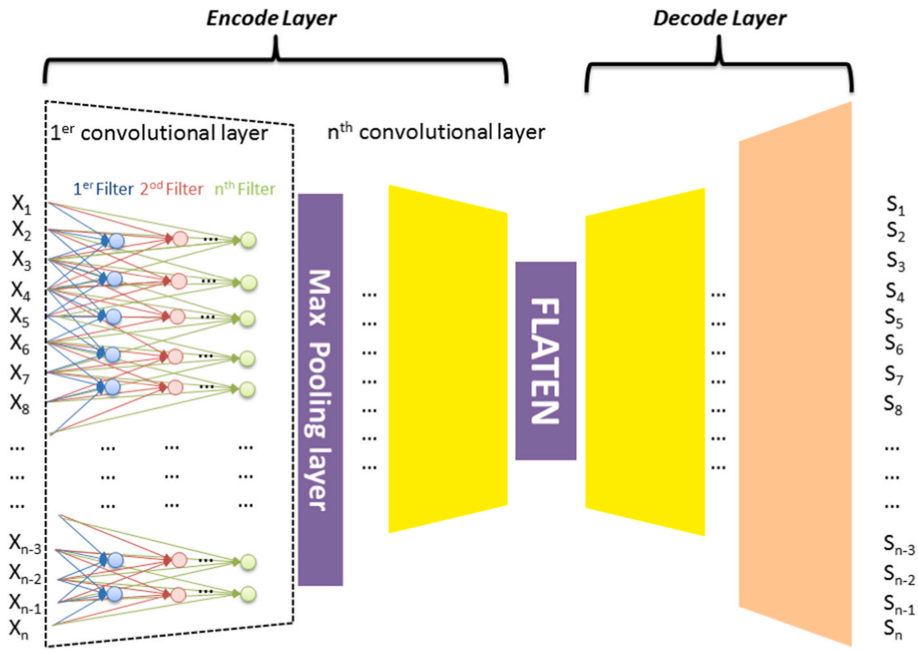

Fig. 1. An illustrative depiction of numerical tools for Auto Encoding is displayed. On the left, it corresponds to a Convolutional Neural Network topology with convoluted filters, followed by a flatten layer and an expansive area.

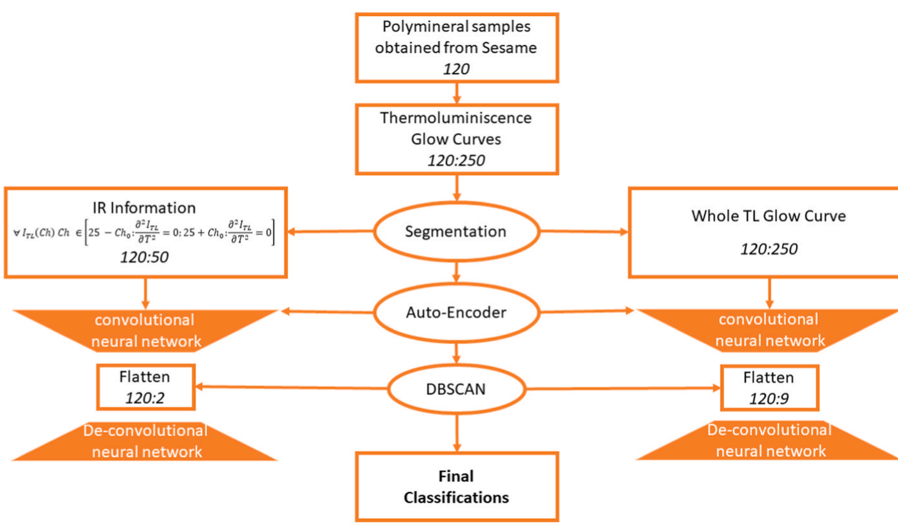

Fig. 2. Flow diagram of the experimental methodology.

control. The TL curve analysis provides useful information on the irradiation treatment, while AI methods offer the potential for automation and optimization of the analysis process. Together, they provide a streamlined and accurate way of testing irradiated foods, which is crucial for ensuring consumer safety and compliance with regulatory requirements.

The aim of AI is to replicate human cognitive abilities through mathematical algorithms, which enable the analysis of large volumes of experimental data. One of the most common AI methods are unsupervised algorithms, which are useful for analyzing data sets that cannot be pre-classified due to insufficient technical or human resources, as reported by Chi-Kuang and Hsuan-Ming (2021). These deep learning techniques have the ability to learn from experimental data sets through self-learning, as demonstrated by Haykin (2010, 2006) (Haykin, 2010; Bishop and Nasrabadi, 2006), respectively.

This paper focuses on the development of an AI numerical method for conducting a blind test to distinguish between irradiated and non-irradiated sesame samples. The method employs TL glow curves obtained from polymineral phases adhered to sesame seeds, along with activation energies estimated through the IR method. Variations in the physicochemical properties of the samples can result in deviations in the shape of TL glow curves. To address this, AI-based mathematical algorithms were employed. Two complementary AI approaches were utilized: (i) deep learning algorithms, such as auto-encoders, were used to reduce the number of variables needed to solve the problem by compressing the data; and (ii) classifiers, such as DBSCAN, were employed to identify areas of high point density and distinguish them from areas of low density. These methods were developed, trained, and implemented using freely available software tools based on Python code and the Google Colab programming environment. This allowed for efficient processing of large volumes of data.

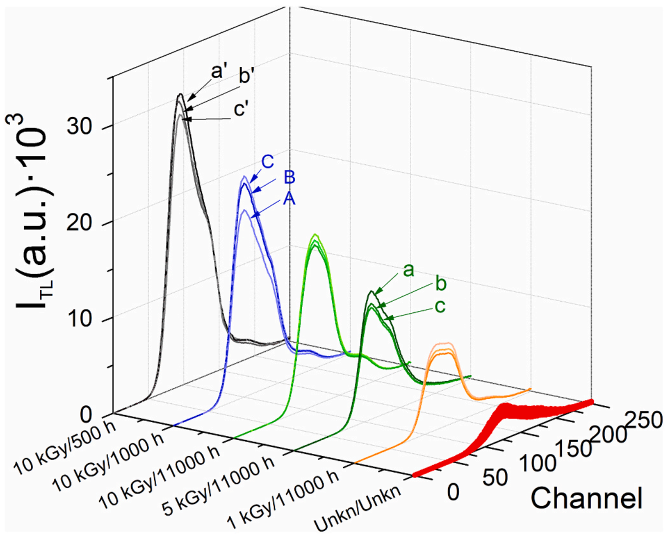

Fig. 3. TL glow curve 3D. Full lines are related to TL glow curves obtained from polymineral samples previously irradiated. Those curves labelled (A, B, C; a, b, c; a', b', c') will be utilized to test the quality of the techniques in differentiating groups with identical thermal history and radiation exposure.

2. Materials and methods

2.1. Sample preparation and measurements

Polymineral phases adhered to the surface of sesame are isolated by means of the different densities of inorganic and organic phases as described in (Benitez et al., 1994). The TL glow curves were obtained using an automated Risø TL reader model TL DA-12 provided with an EMI 9635 QA photomultiplier. TL glow curves were recorded through a blue filter (a FIB002 of the Melles-Griot Company) with peak transmittance is 60%. The TL reader is provided with a $^{90}Sr/^{90}Y$ source with a dose rate of 0.010 Gy/s calibrated against a ^{137}Cs photon source in a secondary standard laboratory. All the TL measurements were obtained using a linear heating rate of 5 °C/s to 500 °C in N_2 atmosphere and the background (due to the incandescence and electronic noise of the reader) was directly subtracted from the TL data after a second TL readout of each aliquot.

2.2. Numerical method

In scenarios where the state of irradiation samples is unknown, unsupervised AI methods can be effectively optimized for clustering and analysing experimental measurements. These methods provide a means to extract patterns and structure from the data without prior knowledge or guidance. By leveraging advanced algorithms, unsupervised AI techniques can identify inherent relationships and similarities within the dataset, enabling the grouping of samples into clusters based on shared characteristics. This approach proves particularly valuable when dealing with complex and large-scale datasets, allowing for a

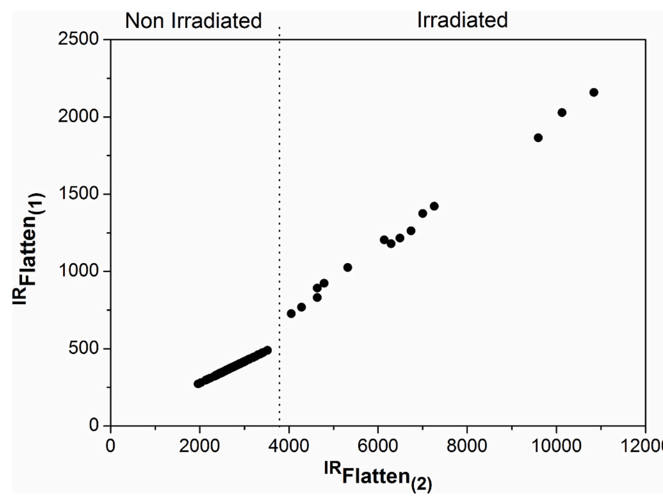

Fig. 5. Areas of high density of points using the bi-dimensional Flatten Layer Vector obtained from AE method using segmented TL curves.

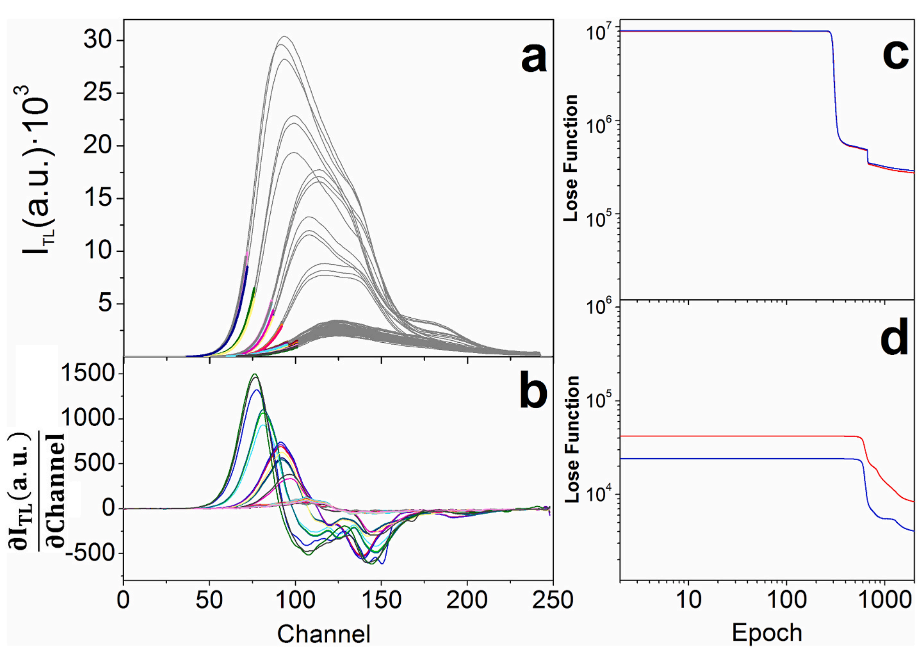

Fig. 4. a) TL glow curves with intensity highlighting the initial rise channels. b) The first derivative of the TL glow curves. c) Results of the training stage using the whole TL glow curves. The blue line represents the Loss Function evaluated with the training dataset, while the red line represents the Loss Function evaluated with the testing dataset. d) Results of the training stage using the Initial Rise TL glow curves.

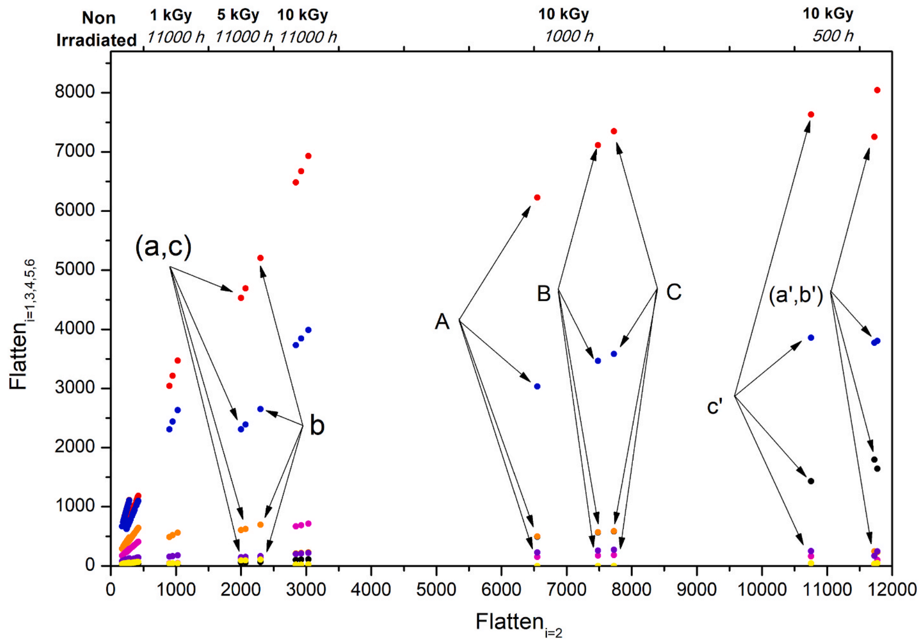

Fig. 6. Flatten Layer Vector. Main vertical axe is related with components 2 (Black circle dot), 3 (Red circle dot) and 4 (Green circle dot t) values.

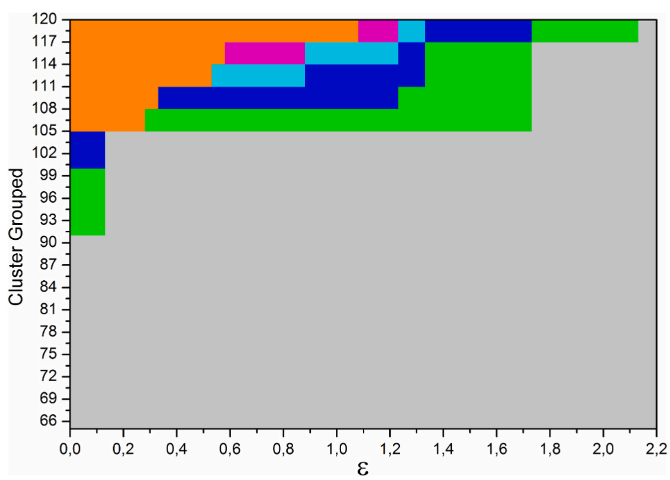

Fig. 7. Results of the DBSCAN algorithm. Cluster 0 (light gray); Cluster 1 (green); Cluster 2 (blue); Cluster 3 (light blue); Cluster 4 (magenta); Cluster −1 (orange).

comprehensive exploration and understanding of the underlying patterns within the data.

2.2.1. Auto-Encoder (AE) algorithm

Auto-Encoders (AE) are a type of unsupervised deep learning method (Partin et al., 2023) that are commonly employed to identify patterns of behaviour within datasets. They use data compression techniques to reduce the size of the dataset while retaining significant information. The architecture of the AE method (Haykin, 2010; Bishop and Nasrabadi, 2006) can be divided into three layers: i) Encoding layer, ii) Flatten layer, and iii) Decoding layer (Fig. 1).

The implemented Encoding layer structure has the function of discovering behavior patterns within each experimental TL glow curve, using a convolutional neural network (CNN) with varying numbers of filters per convolutional layer. All neuronal weights ${}^{n}\omega_{ij}$ that are related to synaptic relationships between neurons, were optimized during the training stage using gradient reduction methods. Each convolutional layer can be characterized by three primary parameters: i) the number of convolutional filters, ii) the kernel size, which is an integer that specifies the length of the convolution window, and iii) the stride parameter, which is an integer that defines the stride length of the convolution. Similarly, the max-pooling layer can be defined by considering the

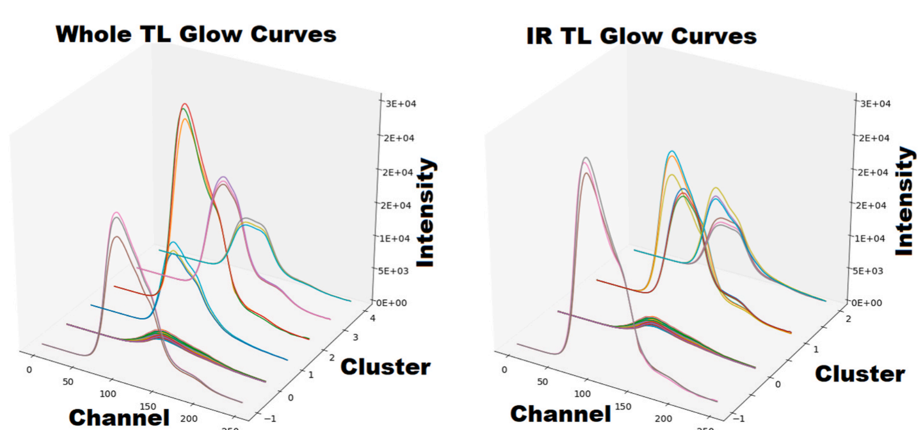

Fig. 8. Results of the no-supervised method implemented using Python Code. Results available for download.

kernel size and stride length values. A first convolutional layer, referred to as Z, was implemented using 32 filters with a kernel size of 3 and a stride parameter of 1. Therefore, these parameters produced 32 × 248 output values, as described in equation (1).

$$Z_{n,j} = {}^{n}F_j\left(\sum_{i=j}^{j+\text{Kernel Size}} {}^{n}\omega_{ij} \times I_{TL\,i} + {}^{n}b_j\right)\Bigg|_{\forall n\in[1,32];\forall j\in[1,248]} \tag{1}$$

The 248 output values obtained from each filter were reduced to 123 by implementing a MaxPooling layer that takes the maximum value among four contiguous values (or window), with a stride of 2.

A second convolutional layer, denoted as X, was introduced with 8 filters using a kernel size of 4 and a stride parameter of 1, resulting in 8 × 120 output values (Eq (2)).

$$X_{d,k} = {}^{d}B_k\left(\sum_{j=k}^{k+\text{Kernel Size}}\left(\sum_{n=1}^{32} {}^{d}\omega_{jk} \times Z_{n,j}\right) + {}^{d}b_k\right)\Bigg|_{\forall d\in[1,8];\forall k\in[1,120]} \tag{2}$$

Another MaxPooling layer was applied with a pool size of 2 and a stride parameter of 2, which reduced the output of each filter to 60 values.

Finally, the last convolutional layer introduced only one filter denoted as F with a kernel size of 60 and a stride of 6. As a result, the flatten layer was reduced to only 9 parameters (Eq (3)).

$$F_l = {}^{l}G\sum_{j=1}^{60}\left(\sum_{d=1}^{8} {}^{d}\omega_j \times X_{d,k}\right) + {}^{l}b\Bigg|_{\forall l\in[1,9]} \tag{3}$$

The deviation obtained between the CNN output value S_i and the true value $I_{TL}(\text{Channel}_i)$ related to experimental data, can be estimated using Lose Function defined as follows (Eq (4)):

$$\text{Lose Function} = \sum_{k=1}^{\text{Epoch}}\sum_{i=1}^{250}\frac{\left({}^{(k)}I_{TL}(\text{Channel}_i) - {}^{(k)}S_i\right)^2}{2} \tag{4}$$

Where the Epoch parameter is related to experimental dataset size (N values), which is divided into two data sub-dataset: i) The first, with a size of 0.70 × N, is used to optimize the values de ${}^{(k)}w_{ij}$ during the training stage. ii) Second is used for testing during the training process. Equation (4) is used to obtain the optimum weight values ${}^{(k)}w_{ij}$, during CNNs training stage using as iterative algorithm based on gradient descent implementing a back propagation method as follows (Eq (5)):

$${}^{(k)}w_{ij_{[t+1]}} = {}^{(k)}w_{ij_{[t]}} - \alpha \bullet \frac{\partial(\text{Lose Function})}{\partial^{(k)}w_{ij}}\Bigg|_{[t]} \tag{5}$$

2.2.2. *Density-based spatial clustering of applications (DBSCAN)*

The unsupervised learning algorithm is based on the detection of areas with high density of points compared to those with low density. In order to identify these areas, it is necessary to estimate the so-called "nuclear points", which are defined as points having at least 'MinPts' number of neighbouring points within a radius ε. Then, the Euclidean distance between datasets obtained from the previously flattened layer is calculated as follows (Eq (6)):

$$\varepsilon_i = \sqrt{\sum_{j=1}^{9}\left(F_i - F_j\right)^2} \tag{6}$$

Densities point zones (or clusters) were grouped taking account both parameters (MinPts, $\varepsilon_i < \varepsilon$) that define the method (Vapnik, 1995).

The research methodology employed in this study is shown in Fig. 2, illustrating the flowchart. 120 TL glow curves were obtained from polymineral sesame samples, with each curve consisting of 250 data channels. The acquired data, organized as a 120 × 250 dimensional matrix, underwent analysis to identify clusters corresponding to distinct irradiation stages.

3. Results and discussion

Fig. 3 shows a representative set of TL glow curves that were acquired from a polymineral phase primarily composed of quartz, feldspars, calcite, gypsum, and clinochlore, as reported by Rodríguez-Lazcano et al. (2013). Such mineralogical composition concerning the type of the minerals does not differ from those isolated from different spices, seasonings and herbs reported in our previous studies (Correcher et al., 1996, Correcher et al., 1998; Benitez et al., 1994, Rodríguez-Lazcano et al., 2013). The TL emission is attributed to mineral phases containing (i) intrinsic defects that play a crucial role in the luminescence process, which are naturally present within the material. They can modify its electronic structure and produce energy levels within the bandgap of the material. When the material is excited with energy (i.e. ionizing radiation), electrons can be promoted to these energy levels, and subsequently release energy in the form of light as they return to their original state. These defects include vacancies appearing when an atom is missing from its regular lattice site or interstitials occur when an atom occupies a site that is usually unoccupied. Thus, Frenkel defects (due to an ion displaced from its lattice site into an interstitial site leaving behind a vacancy defect) and/or Schottky defects (a pair of oppositely charged vacancies is created) play an important role in the TL properties of materials. (ii) Structural defects that are associated with multiple lattice sites and can include dislocations and grain boundaries. Dislocations (linear defects) or twinning planes induce disruptions in the regular arrangement of atoms, while grain boundaries occur at the interface between two grains, or crystal domains, within a material that are also responsible of the TL emission. (iii) Extrinsic defects due to the replacement of an impurity by host atoms within the crystal lattice. Such process can lead to changes in the TL properties of the material. (iv) Surface defects that are induced, for instance, due to chemical reaction (corrosion, dehydration, dihydroxylation, etc.) or radiation-induced defects. The combination of these defects in a polymineral phase gives rise to a very complex glow curves that cannot be easily analysed to determine the TL kinetic parameters. Therefore, the use of the IR method appears as the most suitable one quickly determining the E values that will allow us to discriminate irradiated and non-irradiated samples (Correcher and Garcia-Guinea, 2013). Tests performed on aliquots irradiated randomly with different doses (in the range of 1–10 kGy) and recording the TL glow curve at different elapsed times (from 500 to 11000 h) since the irradiation process confirm this assertion. However, the analytical process can be accelerated considerably if we apply AI algorithms that allow us to process huge amounts of data by applying the appropriate models. For such purpose, the use of unsupervised mathematical methods based on AI algorithms allows for pattern searching behaviour among a large dataset.

In this study, we considered 120 experimental TL glow curves, each with 250 channels, obtained from polymineral phases (quartz, carbonates, feldspars, and clays) of samples adhered to sesame seeds.

Initially, every AI-based mathematical algorithm must be optimized by minimizing the Loss Function (equation (4)) through an iterative gradient descent method (equation (5)). In order to achieve this, the experimental TL curves were randomly divided into two subsets: training and testing data. The testing dataset is used to estimate method oversizing, which along with bias controls, are the two main features that need to be controlled when implementing AI methods. The results of this training stage are presented in Fig. 4, where the Loss Functions (equation (4)) were evaluated after each training epoch. Two segments of each TL curve were utilized as independent variables in the AutoEncoder (AE) method, and these segments can be summarized as follows: (i) The 250 intensity values from the entire TL glow curve and (ii) the intensity values of the TL curve corresponding to the Initial Rise method (McKeever, 1985) (Fig. 4a), in order to establish a correlation with the results reported by Rodríguez-Lazcano et al. (2013).

For every TL glow curve, a dataset was extracted around the maximum of its first derivative curve (Fig. 4b). This dataset was then used to segment the TL curve.

During the training stage, neither of the segmented curve sets showed any divergence between the Loss Function values evaluated with the test data and the training data. Therefore, oversizing issues could be ruled out. These results confirm that the AE method was optimized without bias or oversizing for both the whole TL glow curve (Fig. 4c) and IR (Fig. 4d).

As mentioned above, the aim of the AE method is to reduce the 250 channels of each TL glow curve to the minimum amount of data possible in the Flatten Layer, without losing any information. This is done to increase the efficiency of studying the density of points. If only the intensity values of each TL curve related to the IR method were taken into account as an independent variable for the AE method, then the strangle process of the AE algorithm would result in obtaining a two-dimensional vector in the Flatten Layer, as shown in Fig. 5. This two-dimensional representation is more useful than 250 values per point for human interpretation.

Fig. 5 displays four distinct areas of high point density, with the highest density area being related to the non-irradiated samples. The other samples with different levels of irradiation were clustered in one of the three remaining areas. Therefore, this method is suitable for distinguishing between irradiated and non-irradiated samples, but it may face difficulties in differentiating between samples with various levels of irradiation. On the other hand, when the whole TL glow curve is used as the AE method independent variable, the strangling process is not as efficient as the one described above. Instead of bi-dimensional vectors, nine-dimensional vectors are obtained in the Flatten Layer, which makes the density dot plot less efficient from a human discrimination capability point of view. However, the DBSCAN method may be more efficient in this case. This is because during the heating stage, all the electron capture centres are involved in the formation of each peak, as each trap either releases trapped electrons or acts as sink free electrons depending on the temperature, as numerically demonstrated by Benavente et al. (2020). Therefore, all this information is displayed with different behaviour patterns across the whole TL glow curve.

Fig. 6 displays the density plot of the point using the Flatten Vector values after the training stage. Six distinct areas are clearly differentiated, corresponding to each group of irradiation states.

These results confirm that the information provided by each whole TL glow curve is well correlated with the information given by these nine components. Furthermore, these values can reproduce the within-group homogeneity of TL curves associated with the non-irradiated, irradiated at 1 kGy (11000 h), and 10 kGy (11000 h) clusters. In addition, similarly to the TL curves, the point plot shows differences between TL curve A and TL curves B and C (Fig. 1) within the group of samples irradiated at 10 kGy (1000 h). Similarly, for TL curve c with respect to samples a and b irradiated at 5 kGy (11000 h), and curve c' with a' and b' within the 10 kGy (500 h) group. Finally, the unsupervised DBSCAN algorithm was employed to identify clusters between areas of point density, whose cluster numbers were adjusted when the conditions defining a nuclear point changed. The relationship between the parameter ε (>2.0, 0.025), the number of clusters, and their relation with area size were studied, and the results are presented in Fig. 7.

Only when ε takes values below 2.0, the DBSCAN method is capable of grouping high-density point areas, whose cluster differentiation increases as ε decreases. Once this value is less than 1.1, the first outlier data (represented as cluster −1) appears, initially related to TL glow curves grouped in cluster 2 (Fig. 3). Fig. 7 reveals that the optimal range of ε values for discriminating between irradiated clusters is between 0.6 and 0.9, as all samples can be grouped within one of the six clusters. Additionally, when ε is below 0.6, a strong relationship was observed between the increase in the group of outliers (labelled as cluster −1) and the decrease in the number of groups associated with irradiated samples, until ε drops below 0.3, at which point all data related to irradiated groups are considered outliers. These results also demonstrated the limitations inherent in the DBSCAN algorithm. Specifically, these constraints become evident when the parameter ε assumes extreme values. When ε surpasses 2.0, the algorithm lacks the capacity to discern between irradiated and non-irradiated samples. Conversely, when ε falls below 0.1, this method introduces the potential for differentiation among samples with varying sensitivities within the non-irradiated group. All the AI-based numerical methods that were developed and trained have been implemented using Python code. Libraries such as Matplotlib and TensorFlow were imported to automate the data analysis process, which involved using either the whole TL curve or taking only values associated with the Initial Rise method. The results of the discrimination analysis, shown in Fig. 7, were obtained directly from the code.

Fig. 8 illustrates that both methods are capable of discriminating between irradiated and non-irradiated samples, however, only when the entire TL curve is initially considered, the combined AE-DBSCAN method can differentiate each subset.

4. Conclusions

This blind test demonstrates a practical example of how unsupervised AI methods can be used to analyse previously unexamined data. Both algorithms were able to discriminate between irradiated and non-irradiated Mexican sesame seeds, regardless of whether only the initial rise portion of the TL glow curve or the entire curve was considered. However, when only the initial rise portion was used, complementary analysis methods (such as IR methods) were necessary to discriminate between different irradiation states. The use of AI algorithms can significantly accelerate the analytical process by processing large amounts of data with appropriate models. Unsupervised AI-based mathematical methods are highly advantageous for pattern discovery in large datasets. These approaches entail the comparison of each experimental curve with the whole of the dataset, thereby accommodating the diverse shapes manifested by the TL glow curve. This capability proves particularly crucial when acquiring experimental data from polymineral phases, as the curve shape becomes intricately linked to the minerals present in the food production environment. Therefore, it enables the formulation of a comprehensive methodology for future measurements.

Declaration of competing interest

The authors declare that they have no known competing financial interests or personal relationships that could have appeared to influence the work reported in this paper.

Data availability

Data will be made available on request.

References

Aramu, F., Brovetto, P., Rucci, A., 1966. Activation energy in the NaCl thermoluminescence. Phys. Lett. 23, 308–309. https://doi.org/10.1016/0031-9163(66)90012-6.

Benavente, J.F., Gómez-Ros, J.M., Romero, A.M., 2020. Numerical analysis of the irradiation and heating processes of thermoluminescent materials. Radiat. Phys. Chem. 170, 108671 https://doi.org/10.1016/j.radphyschem.2019.108671.

Benitez, P., Correcher, V., Millan, A., Calderon, T., 1994. Thermoluminescence analysis for testing the irradiation spices. J. Radioanal. Nucl. Chem. 185, 401–410. https://doi.org/10.1007/BF02041311.

Bishop, C.M., Nasrabadi, N.M., 2006. Pattern Recognition and Machine Learning. springer, New York. ISBN-10: 0387310738.

Chi-Kuang, L., Hsuan-Ming, H., 2021. Unsupervised deep learning based image outpainting for dual-source, dual-energy computed tomography. Radiat. Phys. Chem. 188, 109635 https://doi.org/10.1016/j.radphyschem.2021.109635.

Correcher, V., Garcia-Guinea, J., 2013. Potential use of the activation energy value calculated from the thermoluminescence glow curves to detect irradiated food. J. Radioanal. Nucl. Chem. 298, 821–825. https://doi.org/10.1007/s10967-013-2473-3.

Correcher, V., Muniz, J.L., Gomez-Ros, J.M., 1998. Dose dependence and fading effect of the thermoluminescence intensities in gamma-irradiated paprika. J. Sci. Food Agric. 76, 149–155. https://doi.org/10.1002/(SICI)1097-0010(199802)76:2<149::AID-JSFA914>3.0.CO;2-G.

El-Faramawy, N., Sabry, M., Farouk, S., El-Kinawy, M., Mafodda, A., Woda, C., 2023. Preliminary study of lithium tetraborate doped with Cu and in for external dosimetry. Appl. Radiat. Isot. 191, 110533 https://doi.org/10.1016/j.apradiso.2022.110533.

EN, 1788. Thermoluminescence Detection of Irradiated Food from Which Silicate Minerals Can Be Isolated, 2001. European Committee for Standardization, Brussels.

Esmaeili, S., Khanniri, E., Ardestani, S.B., Barzegar, M., Sahari, M., 2023. What are the effects of gamma irradiation, modified atmosphere packaging, and storage on different properties of turmeric essential oil? Radiat. Phys. Chem. 204, 110677 https://doi.org/10.1016/j.radphyschem.2022.110677.

Gu, Y., Wang, M., Zhang, Q., Ge, L., Xu, L., Lu, H., 2022. Accurate-parametric SAR-TL dating protocols for older sediments using quartz. Appl. Radiat. Isot. 181, 110072 https://doi.org/10.1016/j.apradiso.2021.110072.

Haykin, S., 2010. Neural Networks and Learning Machines. PHI Learning Private Limited. ISBN-10: 8120337964.

Lam, S.E., Alawiah, A., Bradley, D.A., Mohd Noor, N., 2017. Effects of time-temperature profiles on glow curves of germanium-doped optical fibre Radiat. Phys. Chem. 137, 56–61. https://doi.org/10.1016/j.radphyschem.2016.02.023.

McKeever, S.W.S., 1985. Thermoluminescence of Solids. Cambridge University Press, London. ISBN-10: 0521268781.

Partin, L., Geraci, G., Rushdi, A., Eldred, M.S., Schiavazzi, D.E., 2023. Multifidelity data fusion in convolutional encoder/decoder networks. J. Comput. Phys. 472, 111666 https://doi.org/10.1016/j.jcp.2022.111666.

Rodríguez-Lazcano, Y., Correcher, V., Garcia-Guinea, J., Cruz-Zaragoza, E., 2013. Gamma radiation-induced thermoluminescence emission of minerals adhered to Mexican sesame seeds. Radiat. Phys. Chem. 83, 15–18. https://doi.org/10.1016/j.radphyschem.2012.09.017.

Souadi, G., Oglakci, M., Kaynar, U.H., Correcher, V., Benavente, J.F., Bulcar, K., Ayvacikli, M., Hiziroglu, A., Topaksu, M., Can, N., Karali, E.E., 2022. Thermoluminescence glow curve analysis and kinetic parameters of Eu doped Li2MoO4 ceramic phosphors. Ceram. Int. 48, 19258–19265. https://doi.org/10.1016/j.ceramint.2022.03.218.

Vapnik, V., 1995. The Nature of Statistical Learning Theory. Springer, New York. ISBN-10: 0387945518.